Dynamic Rupture Models of the 2016 M_L 5.8 Gyeongju, South Korea, Earthquake, Constrained by a Kinematic Rupture Model and Seismic Waveform Data

Seok Goo Song[*1] and Benchun Duan[2]

ABSTRACT

The M_L 5.8 earthquake that jolted Gyeongju in southeastern Korea in 2016 was the country's largest inland event since instrumental seismic monitoring began in 1978. We developed dynamic rupture models of the Gyeongju event constrained by near-source ground-motion data using full 3D spontaneous dynamic rupture modeling with the slip-weakening friction law. Based on our results, we propose two simple dynamic rupture models with constant strength excess (SE) and slip-weakening distance (D_c) that produce near-source ground-motion waveforms compatible with recorded ones in the low-frequency band. Both dynamic models exhibit relatively large stress-drop values, consistent with previous estimates constrained by source spectrum analyses. The fracture energy estimates were also larger than those predicted by a scaling relationship with the seismic moment. The dynamic features constrained in this study by spontaneous rupture modeling and waveform comparison may help understand the source and ground-motion characteristics of future large events in southeastern Korea and thus the seismic hazard of the region.

KEY POINTS

- We derive a physics-based source model of the 2016 Gyeongju earthquake via 3D dynamic simulations.
- The dynamic parameters are constrained by fitting near-source ground-motion waveform data.
- The model shows high stress drop and large fracture energy, important for seismic hazard in the region.

INTRODUCTION

The Korean Peninsula is located on the eastern margin of the Eurasian plate and is not considered a seismically active zone. However, the 2016 M_w 5.5 Gyeongju and 2017 M_w 5.5 Pohang earthquakes that occurred in the southeastern part of the Peninsula raised concerns about the need to accurately estimate the seismic hazards in the Peninsula (Fig. 1). Numerous researchers have extensively studied the point source characteristics of both events (e.g., Hong *et al.*, 2017, 2018; Kim *et al.*, 2017, 2018; Son *et al.*, 2018, 2020; Woo, Kim, *et al.*, 2019; Woo, Rhie, *et al.*, 2019). For the Gyeongju earthquake, a finite-source model was obtained by inverting near-source acceleration data (Uchide and Song, 2018). For the Pohang earthquake, finite-source models were obtained by inverting Interferometric Synthetic Aperture Radar data (Song and Lee, 2019) and near-source seismic data (Cho *et al.*, 2023). Palgunadi *et al.* (2020) performed dynamic rupture modeling for the 2017 Pohang earthquake, focusing on the complex fault geometry of the event. This was the first dynamic modeling attempt for an earthquake in the Korean Peninsula. Understanding the dynamic rupture characteristics of earthquakes is critical for determining the seismic hazard characteristics in a region. In other words, estimated dynamic properties such as stress drop (SD) and fracture energy can be used to understand the source characteristics of future large events and their near-source ground motions. But additional dynamic rupture modeling studies have not yet been done for the events in the Korean Peninsula, including the 2016 Gyeongju earthquake.

In dynamic rupture modeling, motions on the fault, especially temporal source parameters such as rupture and slip velocities, are spontaneously determined by a given initial

1. Geologic Hazards Division, Korea Institute of Geoscience and Mineral Resources, Daejeon, Republic of Korea, https://orcid.org/0000-0002-6603-1542 (SGS);
2. Department of Geology and Geophysics, Texas A&M University, College Station, Texas, U.S.A., https://orcid.org/0000-0003-2622-3811 (BD)

*Corresponding author: sgsong@kigam.re.kr

Cite this article as Song, S. G., and B. Duan (2023). Dynamic Rupture Models of the 2016 M_L 5.8 Gyeongju, South Korea, Earthquake, Constrained by a Kinematic Rupture Model and Seismic Waveform Data, *Bull. Seismol. Soc. Am.* **XX**, 1–16, doi: 10.1785/0120230099

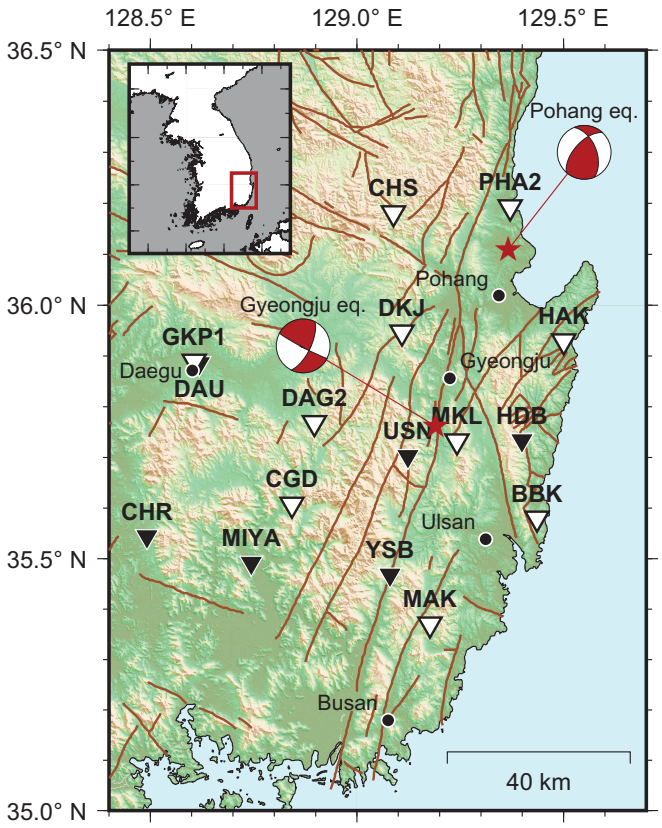

Figure 1. The study area with major fault lines and two recent major earthquakes in the region, that is, the 2016 Gyeongju and 2017 Pohang earthquakes. The inset shows the location of the study area in the Korean Peninsula. The star and the focal mechanism plot indicate the epicenter and the faulting mechanism of the Gyeongju and the Pohang event, which are extracted from Son *et al.* (2018) and Son *et al.* (2020), respectively. Seismic stations in the study area are shown as triangles. Open triangles are used in the study for waveform comparison, and filled triangles are excluded for various reasons (see Results section for details).

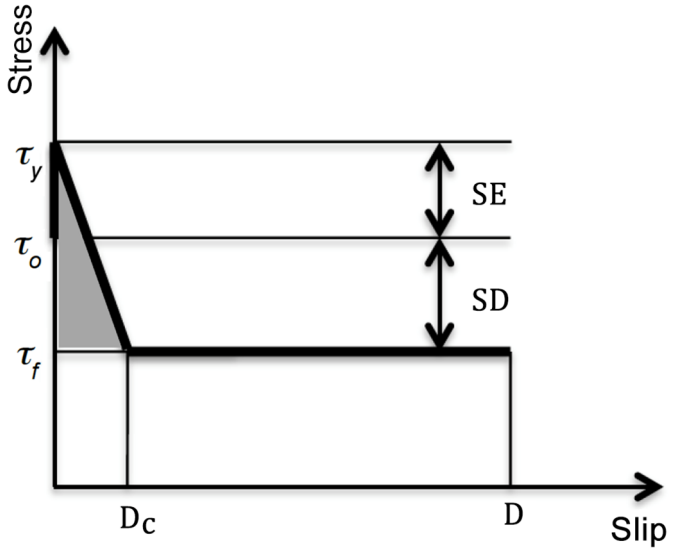

Figure 2. Schematic showing the slip-weakening friction law (Andrews, 1976; Day, 1982) with the following notation: initial stress (τ_o), yield stress (τ_y), final stress (τ_f), slip-weakening distance (D_c), slip, stress drop (SD), and strength excess (SE).

stress field and a friction law (e.g., Ramos *et al.*, 2022). Thus, dynamic rupture modeling is an important tool for understanding earthquake source processes. Recently, well-verified 3D modeling schemes and high-performance computing capabilities have enabled researchers to investigate the dynamic rupture characteristics of earthquakes on a realistic 3D scale. However, constraining dynamic source parameters using full waveform inversion approaches may be difficult because the dynamic source parameters used in the modeling have highly nonlinear relationships with ground motions on the surface, and 3D forward modeling is still computationally expensive. Several attempts have been made to overcome these issues by reducing and simplifying the model space and improving computational efficiency in forward dynamic modeling (e.g., Peyrat *et al.*, 2001; Carli *et al.*, 2010; Gallovič *et al.*, 2019a,b). However, using a traditional source inversion approach to stably constrain the dynamic source parameters remains difficult. To understand the dynamic features of recent large events, some studies (e.g., Duan, 2010, 2012; Kaneko *et al.*, 2017; Weng and Yang, 2018; Wang *et al.*, 2019; Pitarka *et al.*, 2021; Tinti *et al.*, 2021) have used spontaneous dynamic rupture modeling with certain observational constraints.

In this study, we developed a series of spontaneous dynamic rupture models for the 2016 Gyeongju earthquake by varying both the strength excess (SE) and slip-weakening distance (D_c) within the framework of the slip-weakening friction law. We then compared the synthetic waveforms generated by multiple dynamic rupture models with the recorded waveforms in the near-source region to investigate the event's dynamic rupture characteristics, including both the SD and fracture energy. To perform full 3D dynamic rupture modeling, including synthetic waveform calculations, on a realistic scale, high-performance computing capabilities were used. We expect that this type of study will aid us in understanding the dynamic characteristics of earthquakes that have occurred in the southeastern region of the Korean Peninsula and the seismic hazard characteristics of the region as well.

METHODS

Dynamic rupture modeling is a useful tool for understanding the physical properties of earthquake source processes (e.g., Day, 1982; Olsen *et al.*, 1997). Various numerical modeling schemes have been developed and validated in the scientific community (e.g., Harris *et al.*, 2009, 2018). We used the slip-weakening friction law to control the frictional behavior on a fault plane during the rupture process, as shown in Figure 2 (Andrews, 1976; Day, 1982). The critical D_c is the main parameter controlling the decay of traction on the fault when the shear stress on the fault exceeds the yield stress (τ_y)

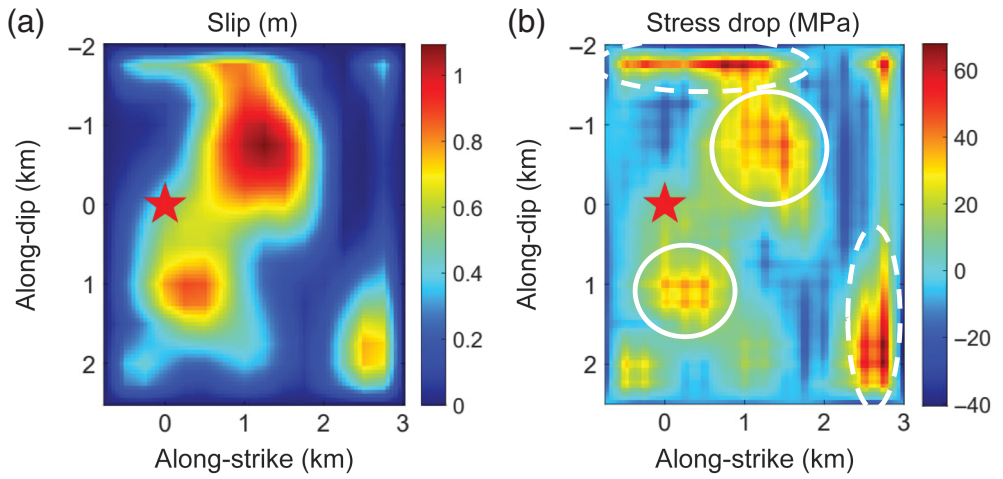

Figure 3. (a) Slip distribution from a kinematic model of the Gyeongju earthquake (Uchide and Song, 2018); and (b) SD distribution computed from the slip using the Okada (1992) method. The red stars indicate the nucleation point, that is, hypocenter location.

and the fault starts slipping. The shear stress on the fault then decays linearly from the τ_y to the final stress (τ_f) since the fault slip reaches the critical slip-weakening distance. Subsequently, it remains at the τ_f level. It is a relatively simple friction law that has been widely used in the dynamic rupture modeling community (e.g., Ramos *et al.*, 2022). Both SD and fracture energy, the two dynamic parameters we focus on in this article, are well defined in the law. The D_c governs the rates at which the shear stress decays and the amount of fracture energy (i.e., shaded area in Fig. 2). Thus, it has a significant impact on the fault motions and the resulting near-source ground motions.

We used a 3D dynamic rupture modeling code, the Support Operator Rupture Dynamics, developed by Ely *et al.* (2009). The code solves the 3D viscoelastic equations of motion by adopting a generalized finite-difference method using logically rectangular hexahedral meshes. The code handles a fault plane using a split-node method in a 3D space (e.g., Day *et al.*, 2005; Dalguer and Day, 2007). It is also parallelized using a message-passing interface, enabling large-scale simulations, and has been well validated in the community (Harris *et al.*, 2009). It has been successfully applied to various dynamic modeling studies (Song and Dalguer, 2013; Song, 2015; Song and Chang, 2021). For high-performance computing with the code, we used a cluster computing system with 1024 cores and 24 TB of memory.

In dynamic rupture modeling with the slip-weakening friction law, three parameters are required as input values—SD, SE, and D_c—as shown in Figure 2. We calculated the static SD distribution from the slip estimate of the kinematic inversion (Uchide and Song, 2018) using Okada (1992) method. Okada presented analytical solutions to compute the deformation (strain), and consequently the stress due to shear faulting, in a homogeneous half-space. Figure 3 shows the slip distribution from a kinematic model of the Gyeongju earthquake (Uchide and Song, 2018) and the SD distribution computed using the Okada method. Two distinctive asperities are recognized in the distribution indicated by solid white circles. The other two white dashed lines could be fault boundary artifacts. The average SD was ~17 MPa when only the non-negative region was considered. The rupture zone was implemented in a computing mesh with fault geometries listed in Table 1. The location and geometry of the fault plane were constrained using estimates from previous studies (Son *et al.*, 2018; Uchide and Song, 2018). We performed multiple sets of dynamic rupture modeling for the 2016 Gyeongju earthquake by perturbing both SE and D_c, with the SD, as shown in Figure 3b. Then we compared the synthetic ground-motion waveforms with the recorded data. Thus, certain aspects of the dynamic rupture characteristics of the Gyeongju event can be inferred, although a more detailed full dynamic inversion is reserved for future research.

Regarding both the SE and the D_c, we assumed constant values for the entire rupture area and tested several values by trial and error to estimate an approximate range of values to generate reasonable fault motions, that is, the rupture propagated in which the majority of the slip is inferred from the kinematic rupture model without stopping and did not evolve into a supershear rupture. Finally, as shown in Table 2, we assigned three values to each variable and created nine sets of dynamic models. Table 2 summarizes the additional numerical modeling parameters used in this study. The absolute level of stress is not the primary concern of this study; we assumed constant depth-independent initial shear stress and normal stress on the fault, that is, 120 and 200 MPa, respectively. We used a 1D crustal velocity model developed for the southeastern

TABLE 1
Fault Geometry and Hypocenter Location Used in Dynamic Modeling

Strike, dip, and rake	25°, 70°, and 180°
Length (*L*) and width (*W*)	3.75 and 4.5 km
Nucleation point (from top left)	0.75 and 2.0 km
Focal depth	12.8 km
Epicenter (latitude and longitude)	35.7621 and 129.1903

TABLE 2
Input Parameters Used for Dynamic Modeling

Grid spacing (d*x*, d*y*, d*z*)	50, 50, and 50 m
Number of grids (n*x*, n*y*, n*z*)	4096, 2048, and 4096
Time step (d*t*)	4 ms
Number of time steps (n*t*)	7501
Slip-weakening distance (D_c)	0.05, 0.1, and 0.15 m
Strength excess (SE)	5, 10, and 15 MPa
Time-weakening parameters (radius of nucleation patch R_c, rupture velocity inside the patch V_{rup}, and time-weakening distance inside the patch T_c)	500 m, 2.5 km/s, and 0.2 s

TABLE 3
Crustal Seismic Velocity Model (Kim *et al.*, 2011)

Depth (km)*	*P*-Wave (km/s)	*S*-Wave (km/s)	Density (g/cm^3)
0.0	5.34	3.18	2.59
3.6	5.91	3.52	2.70
12.0	6.44	3.70	2.82
34.0	8.05	4.60	3.31

*Depth to the top of each layer.

region of the Korean Peninsula (Table 3). The grid spacing used in the study was 50 m, which was small enough not only to compute ground-motion waveforms up to 1 Hz but also to ensure that several grid points are in the cohesive zone during rupture processes, which is required to stably implement the slip-weakening friction law in dynamic rupture modeling (Day *et al.*, 2005). We implemented the time-weakening nucleation patch with a radius of 0.5 km. A fixed rupture speed of 2.5 km/s and a critical time of 0.2 s were used within this artificial nucleation patch.

RESULTS

The ground motions generated by the 2016 Gyeongju earthquake were recorded by regional seismic networks operated by the Korea Meteorological Administration and the Korea Institute of Geoscience and Mineral Resources. Figure 1 shows the station locations analyzed in this study. We initially considered 16 stations; however, six stations were excluded from the waveform comparisons for various reasons. Three borehole stations (HDB, YSB, and MIYA) were excluded because their horizontal alignments were unclear. Two stations (USN and CHR) were excluded because of low data quality. One station (DAU) was excluded because of its proximity to another station (GKP1). Because we used acceleration data, we first integrated them to obtain velocity waveforms and performed band-pass filtering with a frequency range of 0.05–1.0 Hz. Because we used 50 m grid spacing in the dynamic simulations, synthetic ground motions were stably obtained for our target frequency band (i.e., 0.05–1.0 Hz). For waveform comparisons, we also computed the ground motions using the kinematic rupture model obtained by Uchide and Song (2018). The comparison of synthetic ground motions obtained using the dynamic and kinematic rupture models is useful. The synthetic ground motions with the kinematic rupture model were calculated using the same velocity model in Table 3 and the *f-k* code (Cotton and Coutant, 1997).

Because we considered three different values for SE and D_c, we used nine different sets of combinations. For the waveform comparisons, we adopted two metrics such as variance reduction and correlation coefficients. Whereas the former may represent the amplitude difference between the two waveforms, the latter may represent waveform similarity. We also considered three different frequency bands, that is, the upper bounds of the band-pass filter were 0.3, 0.5, and 1.0 Hz with the lower bound being the same at 0.05 Hz. Both the variance reduction and correlation coefficients were computed for three different pairs of combinations—recorded data versus dynamic ground motions, recorded data versus kinematic ground motions, and dynamic ground motions versus kinematic ground motions. Tables 4 and 5 show the values of the variance reduction and correlation coefficients. In three models, spontaneous rupture did not occur, that is, the rupture did not grow out of the initial nucleation zone. Therefore, waveform comparison metrics were not provided for these models. As indicated by the bold numbers in Tables 4 and 5, the best waveform-fitting models were observed for two different combinations. The underlined bold numbers indicate the best values for each frequency band. We assign model I for the model of SE = 5 MPa and $D_c = 0.15$ m and model II for the model of SE = 10 MPa and $D_c = 0.1$ m. We chose these two models as representative dynamic rupture models of the Gyeongju earthquake because they produced the best two waveform-fitting results among the nine sets of tested dynamic rupture models. The two models exhibited similar waveform-fitting results in terms of both variance reduction and correlation.

Figures 4 and 5 show the fault motions of the Gyeongju event obtained by dynamic rupture modeling for models I and II, respectively. The static slip distribution in Figure 2 is well reproduced by both models as shown in the figures, though the rupture did not reach the bottom right corner of the fault in model II. We expect that this part of the rupture may be an artifact, even in the kinematic inversion estimate (Uchide and Song, 2018). In model I, the rupture is trapped in the negative SD region, but finally overcomes it and generates a slip near the bottom-right corner of the fault. In both the models, we observed a higher level of similarity between the distributions of the slip and peak slip velocities. Consequently, the high-peak slip velocity regions were located near the two asperities, that is, the white solid circles in Figure 2. Peak slip velocities were obtained after low-pass filtering for each slip velocity function, up to 1 Hz. The slip duration, which is defined as the time required to complete 10%–90% of the total slip, was greatest near

TABLE 4
Variance Reduction

	0.05 m			0.1 m			0.15 m		
SE\D_c	**0.3 Hz**	**0.5 Hz**	**1.0 Hz**	**0.3 Hz**	**0.5 Hz**	**1.0 Hz**	**0.3 Hz**	**0.5 Hz**	**1.0 Hz**
5 MPa									
Data–dynamic	0.34	−0.14	−1.28	0.47	0.09	−0.83	**0.59**	**0.30**	**−0.58**
Data–kinematic	0.72	0.51	0.10	0.72	0.51	0.10	**0.72**	**0.51**	**0.10**
Dynamic–kinematic	0.70	0.44	−0.76	0.84	0.71	0.19	**0.95**	**0.91**	**0.70**
10 MPa									
Data–dynamic	0.45	−0.08	−0.89	**0.63**	**0.28**	**−0.40**			
Data–kinematic	0.72	0.51	0.10	**0.72**	**0.51**	**0.10**			
Dynamic–kinematic	0.73	0.49	−0.03	**0.93**	**0.87**	**0.78**			
15 MPa									
Data–dynamic	0.56	0.14	−0.52						
Data–kinematic	0.72	0.51	0.10						
Dynamic–kinematic	0.84	0.71	0.53						

The bold numbers indicate the best waveform-fitting models that were observed for two different combinations. The underlined bold numbers indicate the best values for each frequency band. D_c, slip-weakening distance; SE, strength excess.

TABLE 5
Correlation Coefficient

	0.05 m			0.1 m			0.15 m		
SE\D_c	**0.3 Hz**	**0.5 Hz**	**1.0 Hz**	**0.3 Hz**	**0.5 Hz**	**1.0 Hz**	**0.3 Hz**	**0.5 Hz**	**1.0 Hz**
5 MPa									
Data–dynamic	0.79	0.57	0.28	0.83	0.66	0.44	**0.87**	**0.73**	**0.53**
Data–kinematic	0.88	0.76	0.58	0.88	0.76	0.58	**0.88**	**0.76**	**0.58**
Dynamic–kinematic	0.92	0.80	0.48	0.96	0.91	0.78	**0.99**	**0.98**	**0.95**
10 MPa									
Data–dynamic	0.78	0.59	0.39	**0.85**	**0.72**	**0.54**			
Data–kinematic	0.88	0.76	0.58	**0.88**	**0.76**	**0.58**			
Dynamic–kinematic	0.90	0.82	0.70	**0.97**	**0.96**	**0.96**			
15 MPa									
Data–dynamic	0.81	0.65	0.48						
Data–kinematic	0.88	0.76	0.58						
Dynamic–kinematic	0.94	0.89	0.87						

The bold numbers indicate the best waveform-fitting models that were observed for two different combinations. The underlined bold numbers indicate the best values for each frequency band. D_c, slip-weakening distance; SE, strength excess.

the nucleation zone in both models and the negative SD region in model I. Figure 6 shows the moment rate functions of the two models, which were similar, except for the relatively long tail of model I. For comparison, the moment-rate function of the kinematic model is also shown. The moment-rate function of the kinematic rupture model spreads out more over the total rupture period. The effective source duration of the dynamic models is ∼0.8 s, whereas that of the kinematic model is ∼1.2 s. The difference may be reduced or removed using nonuniform SE and/or D_c in dynamic rupture models. However, it appears that the difference does not affect low-frequency ground motions significantly, and we use uniform SE and D_c in this study for simplicity.

Although we did not perform a full dynamic source inversion to produce the best waveform-fitting results with the recorded data, it would be interesting to see how well our two best models produced waveforms that were compatible with the recorded data. Figures 7 and 8 show the waveform comparison for models I and II, respectively, for three different frequency ranges, that is, 0.05–0.3 Hz, 0.05–0.5 Hz, and 0.05–1.0 Hz. In both models, we observe relatively good waveform fitting for the frequency range of 0.05–0.3 Hz. We began to see wiggles above 0.3 Hz that were not explained by the dynamic rupture simulation for several stations, such as HAK, BBK, MAK, GKP1, DKJ, and PHA2. However, interestingly, these wiggles are not explained by the kinematic ground motions, either, which were derived from full kinematic source inversion. This may have originated from local crustal velocity heterogeneities, which were not accounted for in the 1D velocity model in Table 3. Because the Gyeongju event

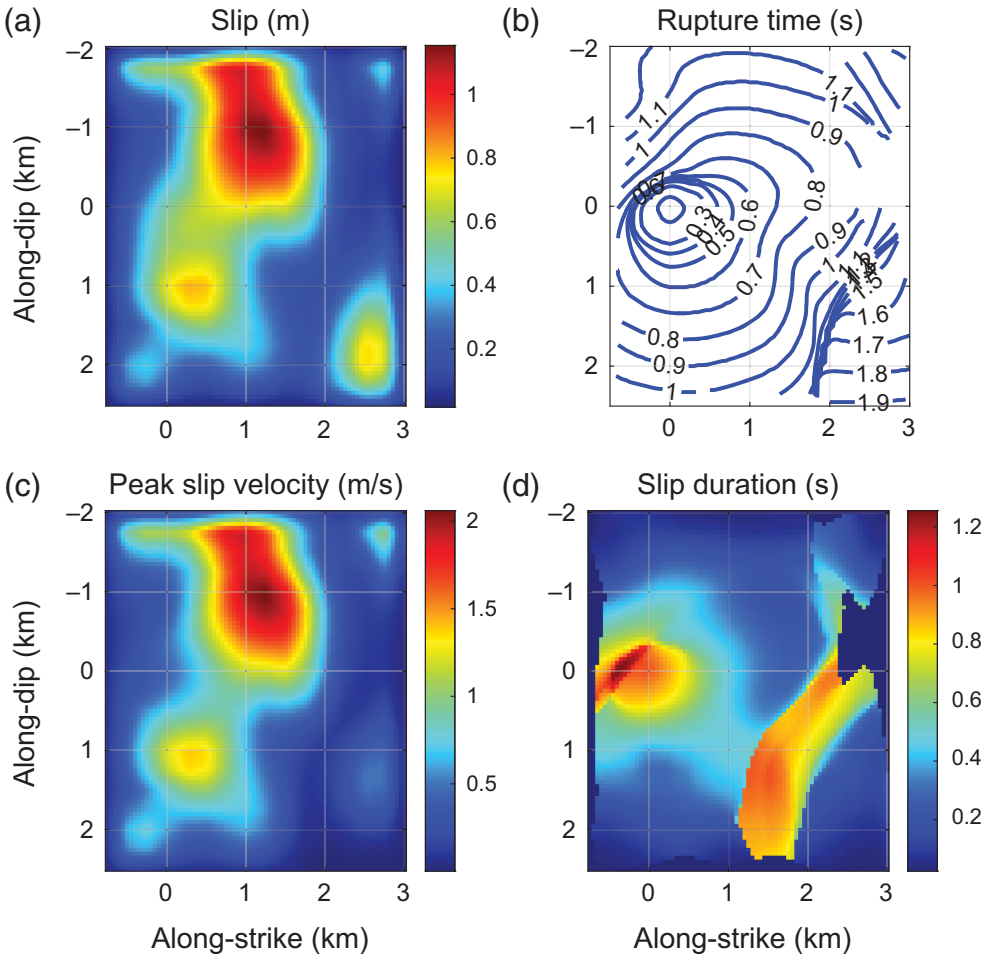

Figure 4. Fault motions derived from dynamic model I. (a) slip (m), (b) rupture time (s), (c) peak slip velocity (m/s), and (d) slip duration (s).

has relatively simple and planar fault geometry (Son *et al.*, 2018; Uchide and Song, 2018), the complex fault geometry effect may not be significant in low-frequency (<1 Hz) waveforms.

Figure 9 shows the distribution of the fracture energy for the two models. The input SD in Figure 3b was used for the fracture energy calculation, and the zero-slip zone in dynamic modeling was also excluded in the calculation. The fracture energy distribution pattern was similar because the same heterogeneous input SD in Figure 3 was used, and both the SE and D_c are constants. Guatteri and Spudich (2000) demonstrated that it might be very difficult to constrain both SE and D_c individually using recorded ground-motion data because of the strong tradeoffs between them. They concluded that the fracture energy may be more stably constrained by waveform inversions. It is interesting to see that two different dynamic models, that is, one with a large D_c (= 0.15 m) and small SE (= 5 MPa) and the other with a small D_c (= 0.1 m) and large SE (=10 MPa), produce a relatively similar level of ground-motion waveform fit to the recorded data in our study. The mean fracture energy calculated only for the nonnegative SD region is 1.51 and 1.25 MJ/m^2, respectively.

DISCUSSION

Although full dynamic source inversion was not performed in this study, multiple sets of dynamic rupture models were created by perturbing both the SE and D_c. The calculated waveforms were then carefully compared with the recorded waveforms for different frequency bands. We also considered the ground motions calculated using the kinematic rupture model for waveform comparison. It is encouraging that we observed good waveform fitting in the low-frequency band, that is, 0.05–0.3 Hz, without full dynamic source inversion. The fitting was relatively good even in the frequency band of 0.05–0.5 Hz. It should also be noted that the dynamic ground motions exhibit very good waveform similarity with the kinematic ground motions up to 1.0 Hz, implying that the waveform dissimilarity between the dynamic ground motions and the recorded ones could be attributed to the 1D crustal velocity model used in the study rather than the dynamic source models themselves. Full dynamic source inversion may be desirable, but in the frequency band of 0.05–1.0 Hz, the detailed features of dynamic parameters may not play a significant role in waveform fitting. We believe that we can obtain a reasonable range of dynamic rupture models that produce waveform similarity in the low-frequency band (< 1 Hz) using forward dynamic rupture modeling.

The SD of the Gyeongju event is relatively large. The mean SD calculated in the nonnegative SD region of Figure 3 was 16.5 MPa. Son *et al.* (2018) provided an estimate of 12.7 MPa by analyzing the source spectrum derived from *S* phases, and Chai *et al.* (2020) provided an estimate of 8.3 MPa using coda-based methods. They also in general agreed that the SD estimates for tectonic earthquakes in this region were relatively large. We used a relatively simple arithmetic mean SD calculation method in this study, although more sophisticated methods with various weighted schemes were proposed (Noda *et al.*, 2013; Wang and Day, 2017). We demonstrated that dynamic rupture models with relatively large SDs and fracture energies can produce near-source ground-motion waveforms

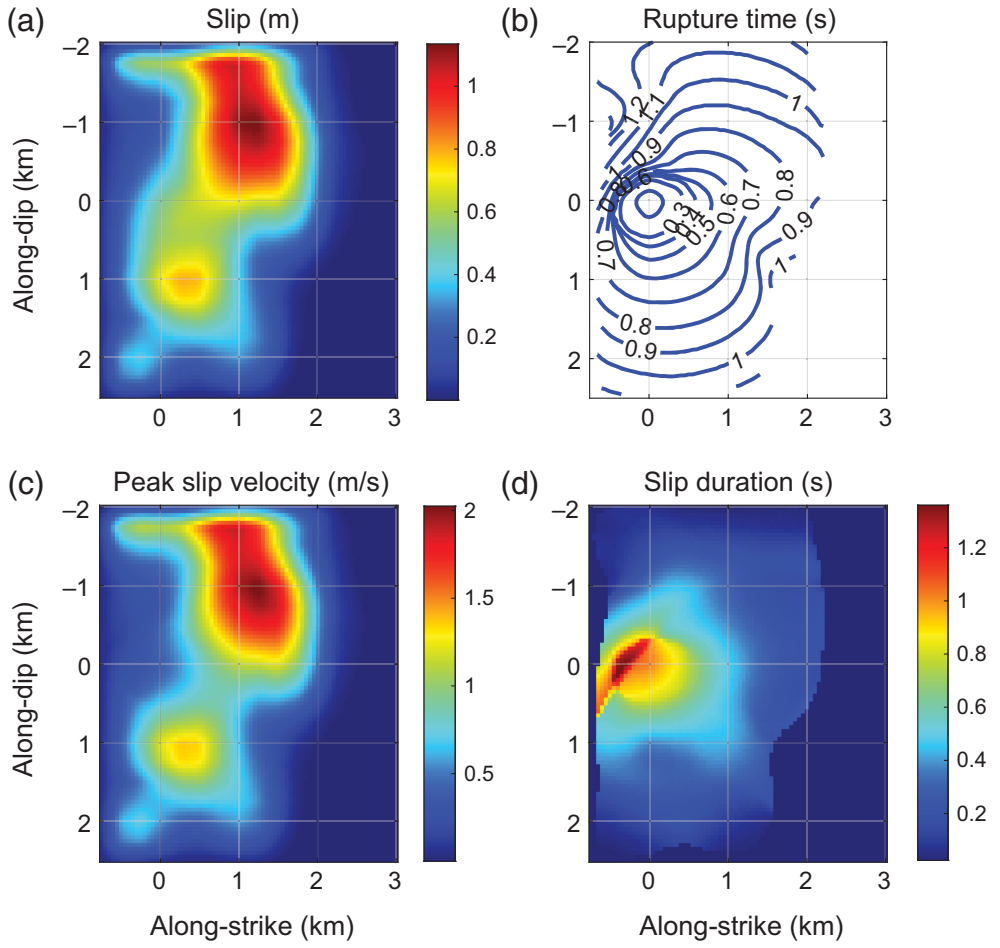

Figure 5. Fault motions derived from dynamic model II. (a) slip (m), (b) rupture time (s), (c) peak slip velocity (m/s), and (d) slip duration (s).

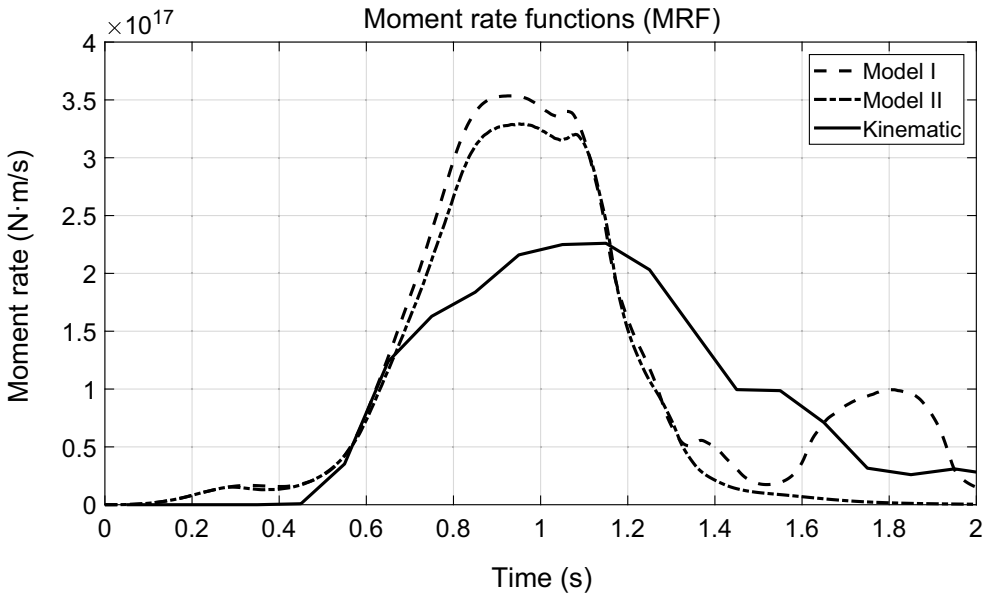

Figure 6. Moment rate functions.

compatible with recorded ones in the low-frequency band. SD is one of the most important source parameters and is often estimated using source spectra (Allmann and Shearer, 2009). However, Brune (1970) SD model often triggers arguments regarding its physical basis, and its estimates are highly variable because of their dependency on the cube of corner-frequency estimates (Atkinson and Beresnev, 1997). We believe that it is valuable to constrain the SD of the Gyeongju earthquake using dynamic rupture modeling in addition to classical source spectrum–based approaches (Son *et al.*, 2018; Chai *et al.*, 2020). Of course, we used the input SD computed from the kinematic slip model by the Okada method and did not perturb the SD distribution in this study. Nevertheless, we compared resulting synthetic waveforms from the dynamic rupture models with the recorded ones and demonstrated that the input SD model produces the synthetic waveforms consistent with the recorded ones.

Ide and Takeo (1997) derived constitutive relations for the 1995 Kobe, Japan, earthquake, by solving elastodynamic equations, given a spatiotemporal slip distribution on the fault plane. Causse *et al.* (2014) adopted the same approach to analyze a set of kinematic source models and derived a fracture energy scaling relation with the seismic moment and average slip (Fig. 10). Based on the scaling relations, the Gyeongju earthquake is expected to have mean fracture energy of 0.58 MJ/m^2 against seismic moment and 3.25 MJ/m^2 against average

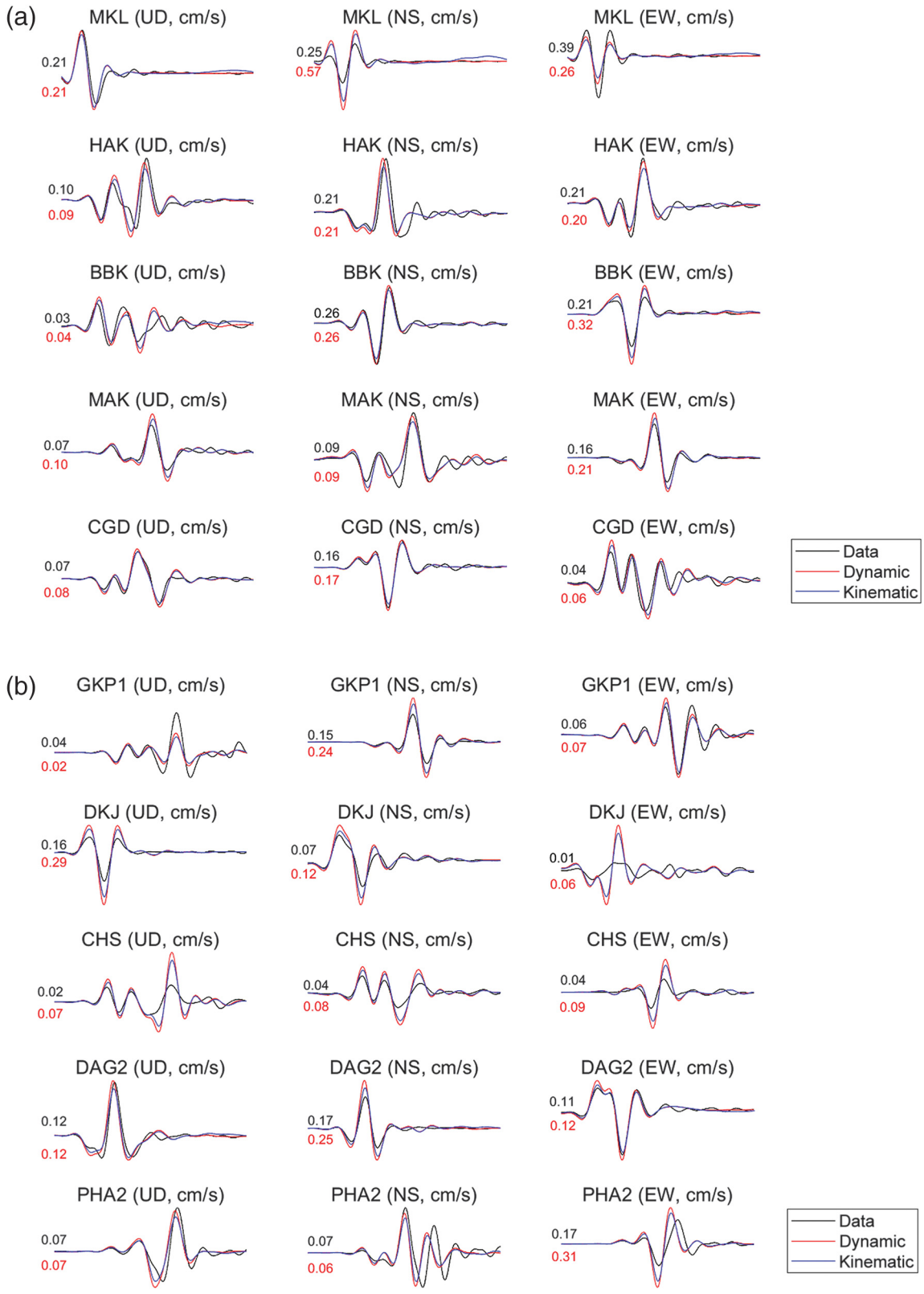

Figure 7. (a,b) Waveform comparison (0.05–0.3 Hz) for model I. The black and red numbers at the beginning of each waveform indicate the maximum amplitude of both recorded waveforms and synthetic waveforms from dynamic rupture modeling. (c,d) Waveform comparison (0.05–0.5 Hz) for model I. (e,f) Waveform comparison (0.05–1.0 Hz) for model I. (*Continued*)

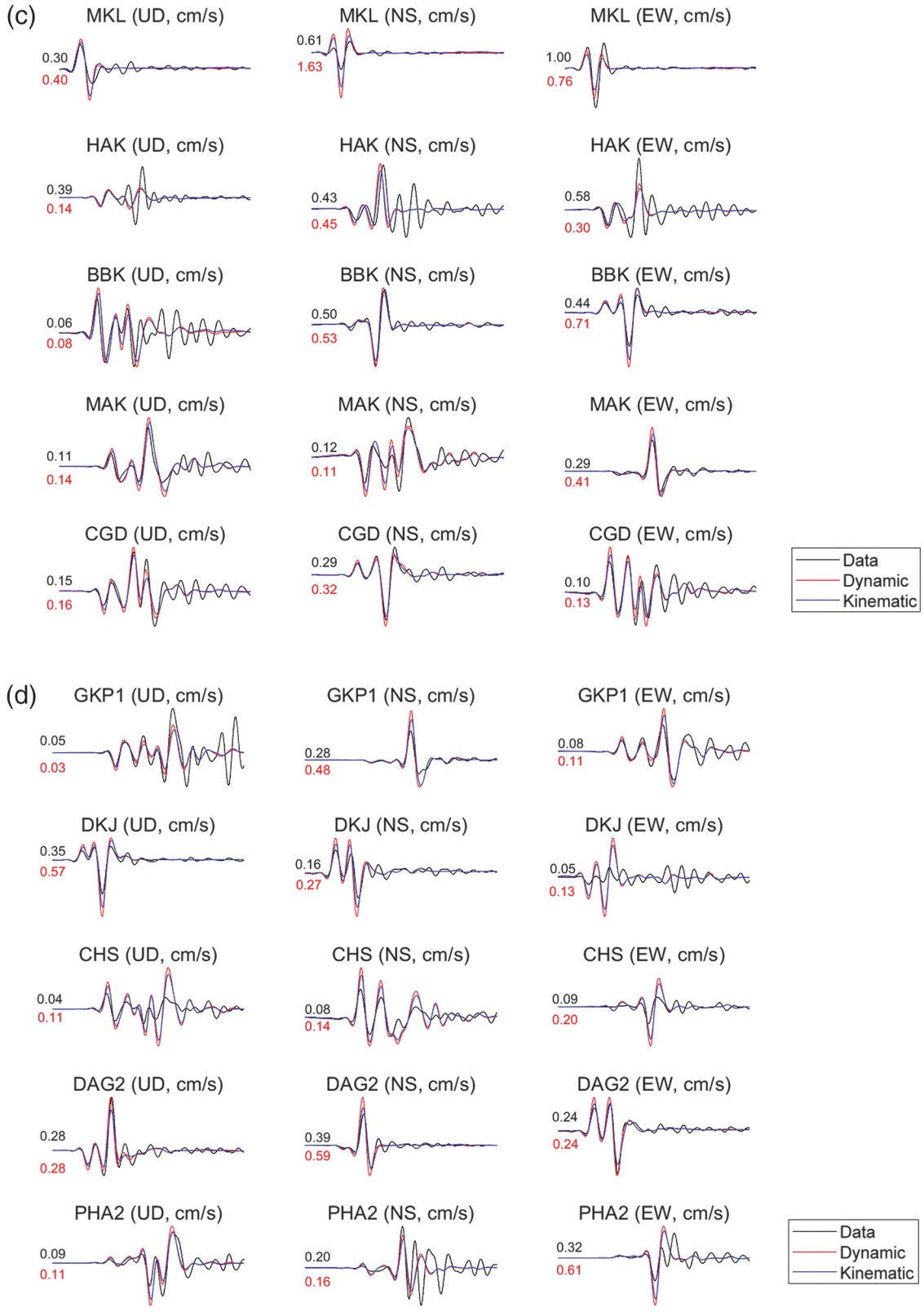

Figure 7. Continued

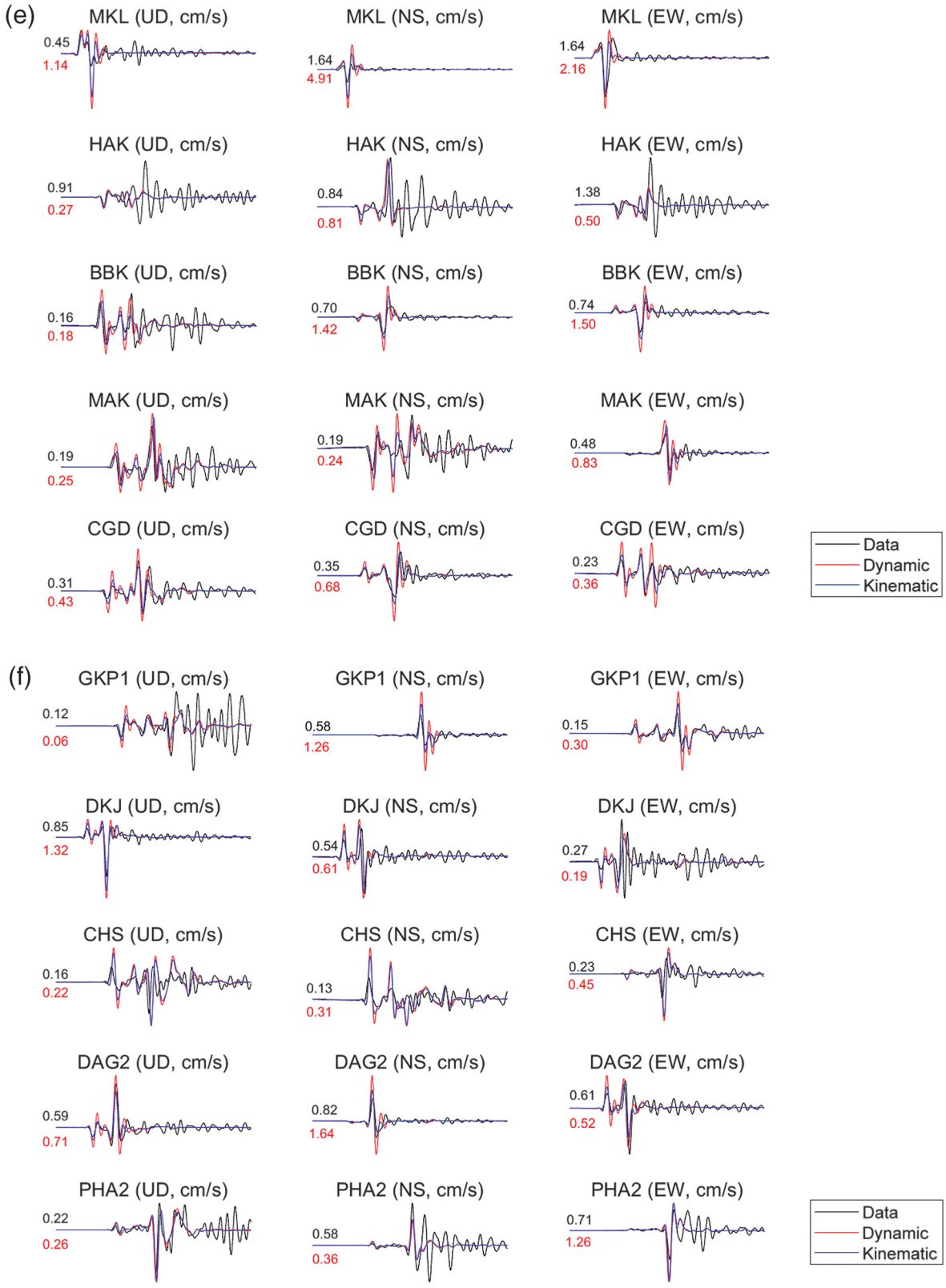

Figure 7. Continued

Figure 8. (a,b) Waveform comparison (0.05–0.3 Hz) for model II. (c,d) Waveform comparison (0.05–0.5 Hz) for model II. (e,f) Waveform comparison (0.05–1.0 Hz) for model II. (*Continued*)

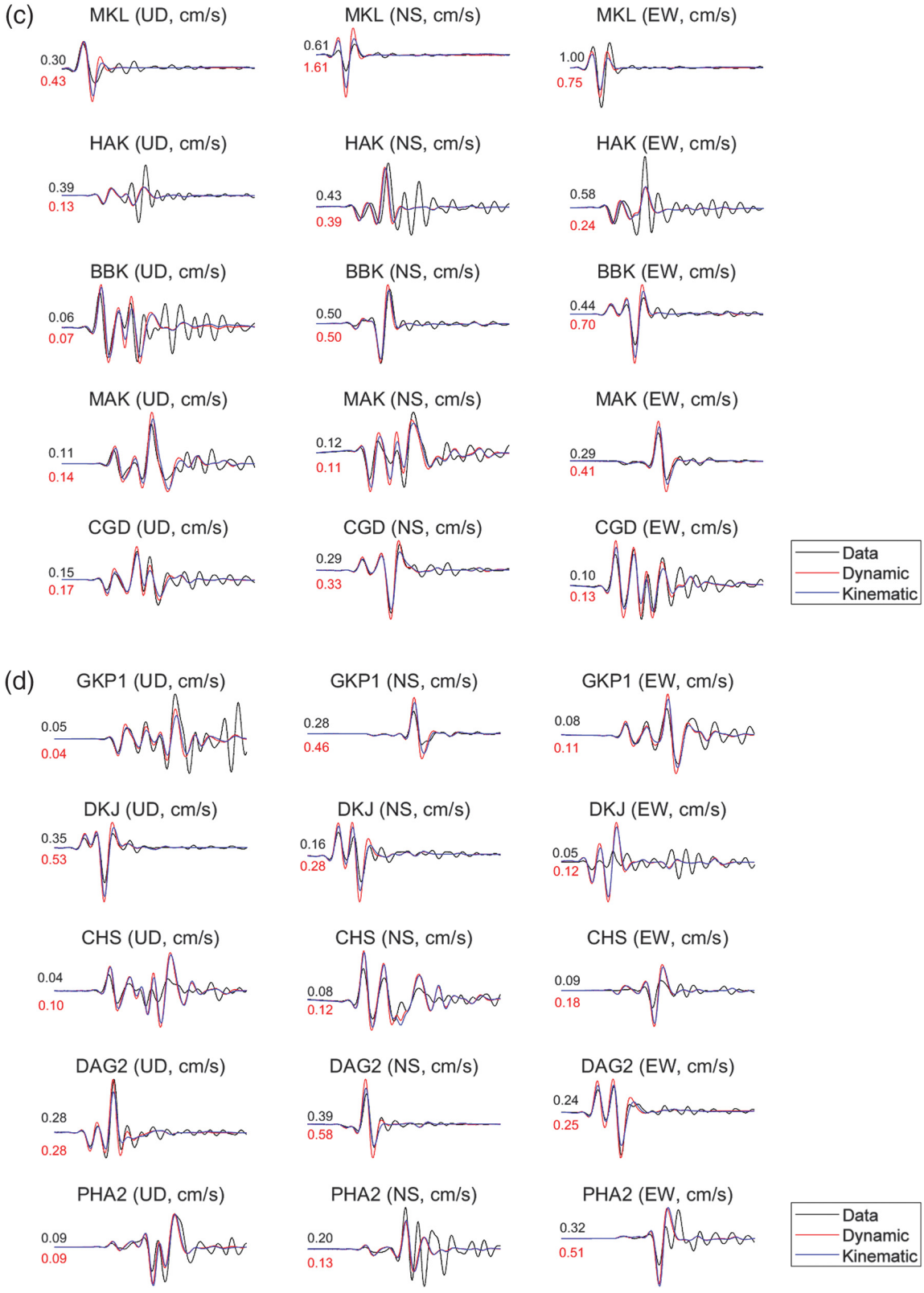

Figure 8. Continued

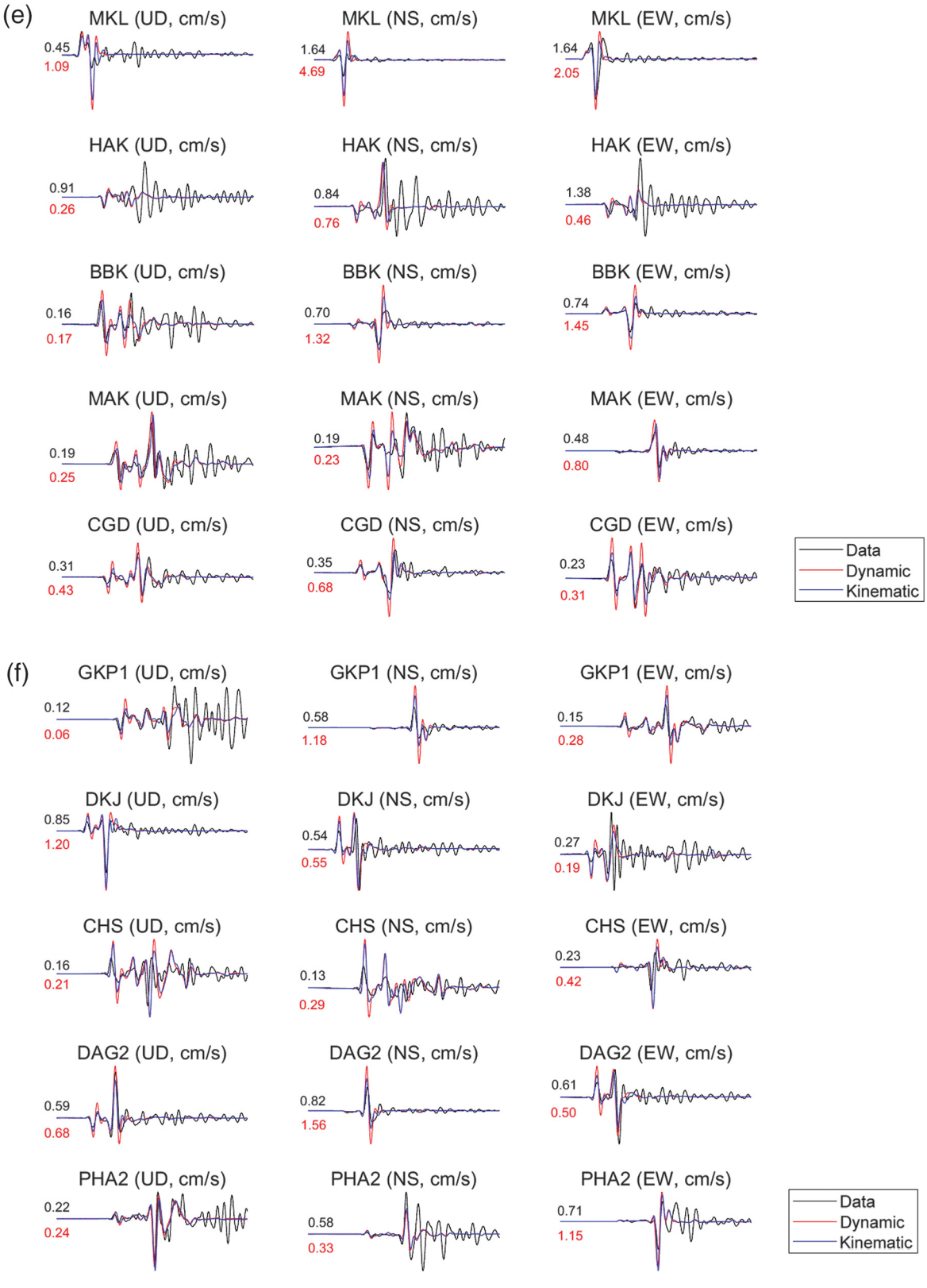

Figure 8. Continued

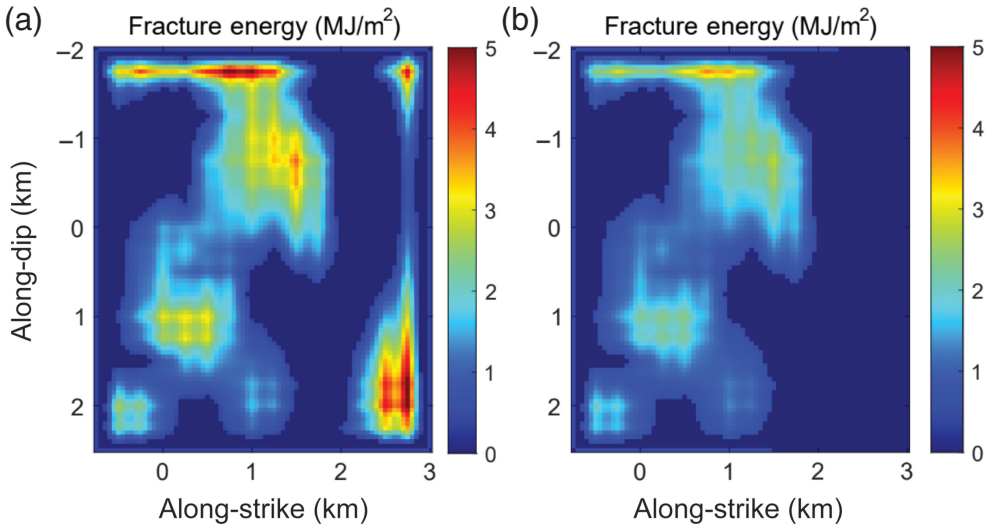

Figure 9. Fracture energy distributions for (a) model I and (b) model II.

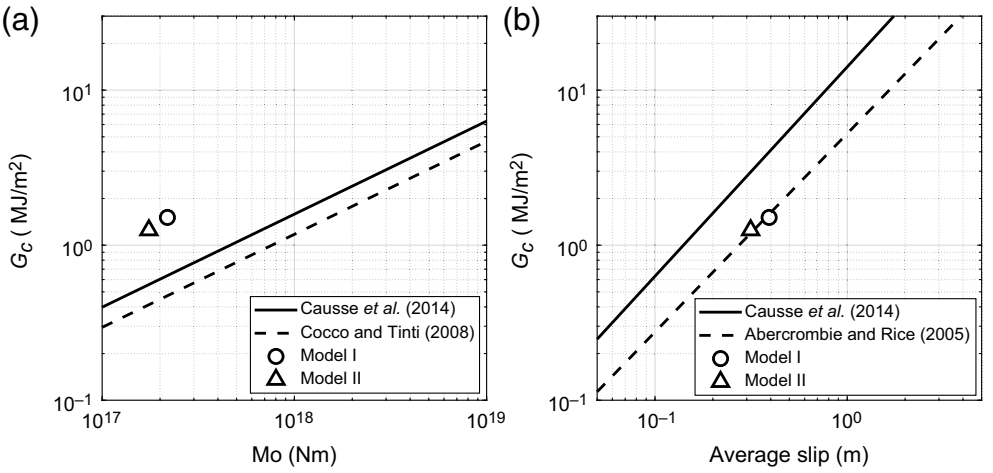

Figure 10. Fracture energy scaling. Fracture energy with (a) seismic moment and (b) average slip. The circle and triangle indicate the fracture energy estimates of our dynamic rupture model I and model II, respectively.

slip. Our estimates of the fracture energy for model I (1.51 MJ/m^2) and model II (1.25 MJ/m^2) were slightly larger than the estimate of the scaling relation with seismic moment and smaller than the estimate of the scaling relation with average slip. This pattern is preserved for the scaling relation of fracture energy against seismic moment even when we added additional scaling relations (e.g., Abercrombie and Rice, 2005; Cocco and Tinti, 2008). Our fracture energy estimates are consistent with the estimates of Abercrombie and Rice (2005) for the scaling relation against average slip. Mai *et al.* (2006) also derived a fracture energy scaling relation, but we excluded it in our analysis because they analyzed a set of forward dynamic rupture models rather than inferring dynamic parameters directly. We believe that this observation is primarily linked to the fact that the Gyeongju earthquake had larger mean SD and mean slip, given its seismic moment. Fracture energy is a relatively unknown parameter in seismic source analyses, but it is crucial in determining the characteristics of the earthquake rupture process, particularly the characteristics of temporal source parameters such as rupture velocity and slip velocity, which significantly affect near-source ground-motion characteristics. Thus, understanding the dynamic characteristics of earthquake sources in southeastern Korea is important because they may provide useful information about the source characteristics of future large events in this region and consequently, the strong ground-motion characteristics generated by these events in the region.

CONCLUSIONS

We performed spontaneous dynamic rupture modeling with the slip-weakening friction law for the 2016 Gyeongju, South Korea, earthquake and proposed two dynamic rupture models (models I and II) for the event, which produced synthetic near-source ground motions, compatible with the recorded ones. We used a full 3D dynamic rupture modeling code and high-performance computing capability and obtained simple dynamic rupture models with constant SE and D_c, constrained by near-source ground-motion data in the low-frequency band (< 1 Hz) without full dynamic source inversion. The dynamic rupture models indicated that the Gyeongju event had relatively larger SD and fracture energy estimates. The dynamic source characteristics of the Gyeongju event are important to understand because they provide useful information for predicting the strong ground-motion characteristics of future events that may occur in the region. Therefore, these data are useful for advanced seismic hazard assessment in this region.

DATA AND RESOURCES

The ground-motion waveform data used in this study are available upon request to the corresponding author. Figure 1 was made using the Generic Mapping Tools (GMT).

DECLARATION OF COMPETING INTERESTS

The authors acknowledge that there are no conflicts of interest recorded.

ACKNOWLEDGMENTS

The authors would like to thank Associate editor Arben Pitarka, and two reviewers Ruth Harris and Yongfei Wang, for their constructive comments. This work was supported by the Basic Research Project (Number GP2020-027) of the Korea Institute of Geoscience and Mineral Resources (KIGAM), funded by the Korean government (Ministry of Science and ICT). The authors are grateful to both KIGAM and the Korea Meteorological Administration (KMA) for providing ground-motion waveform data for the Gyeongju earthquake. The authors are also thankful to Geoffrey Ely for assisting us with his dynamic rupture modeling code and Takahiko Uchide for providing his Generic Mapping Tools script to plot Figure 1.

REFERENCES

Abercrombie, R. E., and J. R. Rice (2005). Can observations of earthquake scaling constrain slip weakening? *Geophys. J. Int.* **162,** 406–424.

Allmann, B. P., and P. M. Shearer (2009). Global variations of stress drop for moderate to large earthquakes, *J. Geophys. Res.* **114,** no. B13, doi: 10.1029/2008JB005821.

Andrews, D. J. (1976). Rupture velocity of plane strain shear cracks, *J. Geophys. Res.* **81,** 5679–5687.

Atkinson, G. M., andBeresnev, I. (1997). Don't call it stress drop, *Seismol. Res. Lett.* **68,** 3–4.

Brune, J. (1970). Tectonic stress and spectra of seismic shear waves from earthquakes, *J. Geophys. Res.* **75,** 4997–5009.

Carli, S. D., C. Francois-Holden, S. Peyrat, and R. Madariaga (2010). Dynamic inversion of the 2000 Tottori earthquake based on elliptical subfault approximations, *J. Geophys. Res.* **115,** doi: 10.1029/2009JB006358.

Causse, M., L. A. Dalguer, and P. M. Mai (2014). Variability of dynamic source parameters inferred from kinematic models of past earthquakes, *Geophys. J. Int.* **196,** 1754–1769.

Chai, G., S.-H. Yoo, J. Rhie, and T.-S. Kang (2020). Stress-drop scaling of the 2016 Gyeongju and 2017 Pohang earthquake sequences using coda-based methods, *Bull. Seismol. Soc. Am.* **110,** 2047–2057.

Cho, E., J.-U. Woo, J. Rhie, T.-S. Kang, and S.-Y. Baag (2023). Rupture process of the 2017 M_w 5.5 Pohang, South Korea, earthquake via an empirical Green's function method, *Bull. Seismol. Soc. Am.* **113,** 592–603.

Cocco, M., and E. Tinti (2008). Scale dependence in the dynamics of earthquake propagation: Evidence from seismological and geological observations, *Earth Planet. Sci. Lett.* **273,** 123–131.

Cotton, F., and O. Coutant (1997). Dynamic stress variations due to shear faults in a plane-layered medium, *Geophys. J. Int.* **128,** 676–688.

Dalguer, L. A., and S. M. Day (2007). Staggered-grid split-node method for spontaneous rupture simulation, *J. Geophys. Res.* **112,** no. B2, doi: 10.1029/2006JB004467.

Day, S. M. (1982). Three-dimensional simulation of spontaneous rupture: The effect of nonuniform prestress, *Bull. Seismol. Soc. Am.* **72,** 1881–1902.

Day, S. M., L. A. Dalguer, N. Lapusta, and Y. Liu (2005). Comparison of finite difference and boundary integral solutions to three-dimensional spontaneous rupture, *J. Geophys. Res.* **110,** no. B12, doi: 10.1029/2005JB003813.

Duan, B. (2010). Role of initial stress rotations in rupture dynamics and ground motion: A case study with implications for the Wenchuan earthquake, *J. Geophys. Res.* **115,** no. B5, doi: 10.1029/2009JB006750.

Duan, B. (2012). Dynamic rupture of the 2011 M_w 9.0 Tohoku-Oki earthquake: Roles of a possible subducting seamount, *J. Geophys. Res.* **117,** no. B5, doi: 10.1029/2011JB009124.

Ely, G. P., S. M. Day, and J.-B. Minster (2009). A support-operator method for 3-D rupture dynamics, *Geophys. J. Int.* **177,** 1140–1150.

Gallovič, F., Ľ. Valentová, J. P. Ampuero, and A. A. Gabriel (2019a). Bayesian dynamic finite-fault inversion: 1. Method and synthetic test, *J. Geophys. Res.* **124,** 6949–6969.

Gallovič, F., Ľ. Valentová, J. P. Ampuero, and A. A. Gabriel (2019b). Bayesian dynamic finite-fault inversion: 2. Application to the 2016 M_w 6.2 Amatrice, Italy, earthquake, *J. Geophys. Res.* **124,** 6970–6988.

Guatteri, M., and P. Spudich (2000). What can strong-motion data tell us about slip-weakening fault-friction laws? *Bull. Seismol. Soc. Am.* **90,** 98–116.

Harris, R. A., M. Barall, B. Aagaard, S. Ma, D. Roten, K. Olsen, B. Duan, D. Liu, B. Luo, K. Bai, *et al.* (2018). A suite of exercises for verifying dynamic earthquake rupture code, *Seismol. Res. Lett.* **89,** 1146–1162.

Harris, R. A., M. Barall, R. Archuleta, E. Dunham, B. T. Aagaard, J. P. Ampuero, H. Bhat, V. M. Cruz-Atienza, L. A. Dalguer, P. Dawson, *et al.* (2009). The SCEC/USGS dynamic earthquake rupture code verification exercise, *Seismol. Res. Lett.* **80,** 119–126.

Hong, T.-K., J. Lee, W. Kim, I.-K. Hahm, N.-C. Woo, and S. Park (2017). The 12 September 2016 M_L 5.8 midcrustal earthquake in the Korean Peninsula and its seismic implications, *Geophys. Res. Lett.* **44,** 3131–3138.

Hong, T.-K., J. Lee, S. Park, and W. Kim (2018). Time-advanced occurrence of moderate-size earthquakes in a stable intraplate region after a megathrust earthquake and their seismic properties, *Sci. Rep.* **8,** no. 1, 13,331.

Ide, S., and M. Takeo (1997). Determination of constitutive relations of fault slip based on seismic wave analysis, *J. Geophys. Res.* **102,** 27,379–27,391.

Kaneko, Y., E. Fukuyama, and I. J. Hamling (2017). Slip-weakening distance and energy budget inferred from near-fault ground deformation during the 2016 M_w 7.8 Kaikura earthquake. *Geophys. Res. Lett.* **44,** 4765–4773.

Kim, K.-H., J. Kim, M. Han, S. Y. Kang, M. Son, T.-S. Kang, J. Rhie, Y. Kim, Y. Park, H.-J. Kim, *et al.* (2017). Deep fault plane revealed by high-precision locations of early aftershocks following the 12 September 2016 M_L 5.8 Gyeongju, Korea, earthquake, *Bull. Seismol. Soc. Am.* **108,** 517–523.

Kim, K.-H., J.-H. Ree, Y. Kim, S. Kim, S. Y. Kang, and W. Seo (2018). Assessing whether the 2017 M_w 5.4 Pohang earthquake in South Korea was an induced event, *Science* **360**, no. 6392, 1007–1009.

Kim, S., J. Rhie, and G. Kim (2011). Forward waveform modelling procedure for 1-D crustal velocity structure and its application to the southern Korean Peninsula, *Geophys. J. Int.* **185,** 453–468.

Mai, P. M., P. Somerville, A. Pitarka, L. Dalguer, H. Miyake, G. Beroza, S. G. Song, and K. Irikura (2006). Fracture-energy scaling in dynamic rupture models of past earthquakes, in *Earthquakes: Radiated Energy and the Physics of Faulting*, A. McGarr, R. Abercrombie, and H. Kanamori (Editors), Geophysical Monograph Series, Vol. 170, American Geophysical Union, Washington, DC, 283–294.

Noda, H., N. Lapusta, and H. Kanamori (2013). Comparison of average stress drop measures for ruptures with heterogeneous stress change and implications for earthquake physics, *Geophys. J. Int.* **193,** 1691–1712.

Okada, Y. (1992). Internal deformation due to shear and tensile faults in a half-space, *Bull. Seismol. Soc. Am.* **82,** 1018–1040.

Olsen, K., R. Madariaga, and R. J. Archuleta (1997). Three-dimensional dynamic simulation of the 1992 landers earthquake, *Science* **278,** 834–838.

Palgunadi, K. H., A.-A. Gabriel, T. Ulrich, J. A. Lopez-Comino, and P. M. Mai (2020). Dynamic fault interaction during a fluid-injection-induced earthquake: The 2017 M_w 5.5 Pohang event, *Bull. Seismol. Soc. Am.* **110,** 2328–2349.

Peyrat, S., K. Olsen, and R. Madariaga (2001). Dynamic modeling of the 1992 Landers earthquake, *J. Geophys. Res.* **106,** 26,467–26,482.

Pitarka, A., R. Graves, K. Irikura, K. Miyakoshi, C. Wu, H. Kawase, A. Rodgers, and D. Mccallen (2021). Refinements to the Graves-Pitarka kinematic rupture generator, including a dynamically consistent slip-rate function, applied to the 2019 M_w 7.1 Ridgecrest earthquake, *Bull. Seismol. Soc. Am.* **112,** 287–306.

Ramos, M. D, P. Thakur, Y. Huang, R. A. Harris, and K. J. Ryan (2022). Working with dynamic earthquake rupture models: A practical guide, *Seismol. Res. Lett.* **93,** 2096–2110.

Son, M., C. S. Cho, H. K. Lee, M. Han, J. S. Shin, K. Kim, and S. Kim (2020). Partitioned fault movement and aftershock triggering: Evidence for fault interactions during the 2017 M_w 5.4 Pohang earthquake, South Korea, *J. Geophys. Res.* **125,** e2020JB020005, doi: 10.1029/2020JB020005.

Son, M., C. S. Cho, J. S. Shin, H. M. Rhee, and D. H. Sheen (2018). Spatiotemporal distribution of events during the first three months of the 2016 Gyeongju, Korea, earthquake sequence, *Bull. Seismol. Soc. Am.* **108,** 210–217.

Song, S. G. (2015). The effect of fracture energy on earthquake source correlation statistics, *Bull. Seismol. Soc. Am.* **105,** 1042–1048.

Song, S. G., and C. Chang (2021). Dynamic earthquake rupture modeling considering regional crustal stress conditions in southeastern Korea, *Geosci. J.* **25,** 211–222.

Song, S. G., and L. A. Dalguer (2013). Importance of 1-point statistics in earthquake source modelling for ground motion simulation, *Geophys. J. Int.* **192,** 1255–1270.

Song, S. G., and H. Lee (2019). Static slip model of the 2017 M_w 5.4 Pohang, South Korea, earthquake constrained by the InSAR data, *Seismol. Res. Lett.* **90,** 140–148.

Tinti, E., E. Casarotti, T. Ulrich, T. Taufiqurrahman, D. Li, and A.-A. Gabriel (2021). Constraining families of dynamic models using geological, geodetic and strong ground motion data: The M_w 6.5, October 30, 2016, Norcia earthquake, Italy, *Earth Planet. Sci. Lett.* **576,** 117,237.

Uchide, T., and S. G. Song (2018). Fault rupture model of the 2016 Gyeongju, South Korea, earthquake and its implication for the underground fault system, *Geophys. Res. Lett.* **45,** 2257–2264.

Wang, Y., and S. M. Day (2017). Seismic source spectral properties of crack-like and pulse-like modes of dynamic rupture, *J. Geophys. Res.* **122,** 6657–6684.

Wang, Y., S. M. Day, and M. A. Denolle (2019). Geometric controls on pulse-like rupture in a dynamic model of the 2015 Gorkha earthquake, *J. Geophys. Res.* **124,** 1544–1568.

Weng, H. H., and H. F. Yang (2018). Constraining frictional properties on fault by dynamic rupture simulations and near-field observations, *J. Geophys. Res.* **123,** 6658–6670.

Woo, J.-U., M. Kim, D.-H. Sheen, T.-S. Kang, J. Rhie, F. Grigoli, W. L. Ellsworth, and D. Giardini (2019). An in-depth seismological analysis revealing a causal link between the 2017 M_w 5.5 Pohang earthquake and EGS project, *J. Geophys. Res.* **124,** 13,060–13,078.

Woo, J.-U., J. Rhie, S. Kim, T.-S. Kang, K.-H. Kim, and Y. Kim (2019). The 2016 Gyeongju earthquake sequence revisited: Aftershock interactions within a complex fault system, *Geophys. J. Int.* **217,** 58–74.

Manuscript received 11 May 2023
Published online 5 October 2023